InP-Based PIC for an Optical Phased-Array Antenna at 1.06 μm

G. Flamand, K. De Mesel, I. Moerman, *Member, IEEE*, B. Dhoedt, W. Hunziker, *Member, IEEE*, A. Kalmar,
R. Baets, *Senior Member, IEEE*, P. Van Daele, *Member, IEEE*, and W. Leeb

Abstract—In this paper, we have demonstrated the feasibility of a photonic integrated circuit for phase control at a wavelength of 1.06 μm in an optical phased array telescope antenna system.

Index Terms—1.06 μm, phase modulation, photonic integrated circuit.

I. INTRODUCTION

AN INCREASING number of future space projects will make use of optical technologies for a wide range of applications. Stringent requirements on size, weight, and reliability create a need for waveguide-based photonic integrated circuits (PIC's). We have investigated the feasibility of the InGaAsP–InP technology for the realization of a PIC for phase control of optical transmission at 1.06 μm. This PIC is to be integrated in an optical phased telescope array system [1]. A similar PIC based on AlGaAs–GaAs technology has already been reported earlier [2]. In this letter, InGaAsP–InP is preferred over the AlGaAs–GaAs material system because of the better resistance to cosmic radiation of InP and the superior efficiency of InP-based detectors (which, in a next step, will be integrated on the PIC) at the 1.06-μm wavelength.

The optical phased array is planned to act as a receive antenna in a terminal for intersatellite laser communications (in geostationary orbit) (see Fig. 1). The incoming radiation is collected by sub-telescopes, and coupled into single-mode fibers, which feed the PIC inputs. After phase control, the sub-beams are superimposed by 3-dB multimode interference (MMI) couplers, where each coupler has a signal output port nominally carrying its total input power and a control output port where the optical power is minimized. All but one control output ports feed photodetectors with error signals to be minimized (by controlling the phase modulators via a digital control unit), while the remaining signal output port (which is automatically maximized) constitutes the antenna output.

II. DESIGN AND FABRICATION

Efficient waveguiding calls for a core (InGaAsP) material with a bandgap wavelength that needs to be, on one hand,
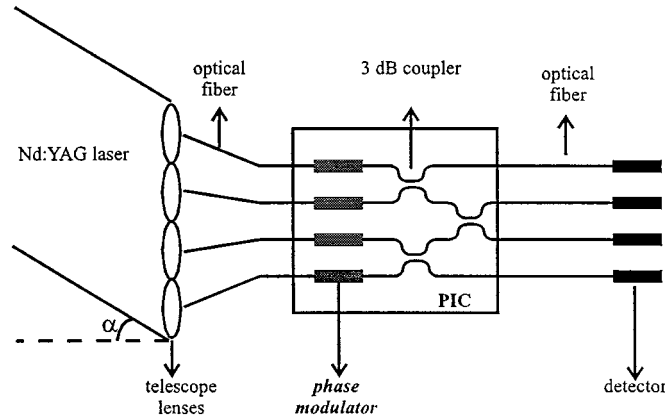
Fig. 1. PIC in optical phased array (receive antenna for intersatellite laser communication).

sufficiently higher than that of the (InP) cladding layers, to obtain a high confinement of the light in the waveguide core, while, on the other hand, it needs to remain appreciably smaller than the wavelength of the guided light to avoid high absorption losses. Since our structure needs to guide Nd : YAG light with a wavelength of 1.06 μm, and the InP-cladding layers have a bandgap wavelength of 0.92 μm, this places very stringent restrictions on the composition of the waveguiding layer. From simulations and a number of waveguide test structures, it was found that the best results can be expected with a waveguiding layer exhibiting a bandgap wavelength between 0.98–1.00 μm (composition between $In_{94.8}Ga_{5.2}As_{11.4}P_{88.6}$ and $In_{93.2}Ga_{6.8}As_{15.0}P_{85.0}$). Further simulation resulted in a layer structure for the PIC, as shown in Fig. 2.

The InGaAsP core layer has a thickness of 700 nm, resulting in monomodal waveguiding for ridge widths up to 1.8–2.2 μm (depending on etch depth). The guiding layer is placed between an n-doped bottom and p-doped top cladding layer, where the latter is separated from the core layer by an undoped cladding layer, in order to reduce additional losses due to the strong absorption of the optical mode in a p-doped layer. This way, we obtain a p-i-n structure, required to make use of the electrooptic and carrier effects to achieve phase modulation [3], [4]. The layer structure is capped with a highly p-doped InGaAs contacting layer.

The above described layer structure was grown using LP-MOVPE. The source materials are PH_3, AsH_3, TMI, and TMG, and H_2S and DEZ for n- and p-doping, respectively. We used an elevated growth temperature of 700 °C, where the higher PH_3-cracking efficiency enables us to use a higher AsH_3 flow than is the case at the standard growth temperature
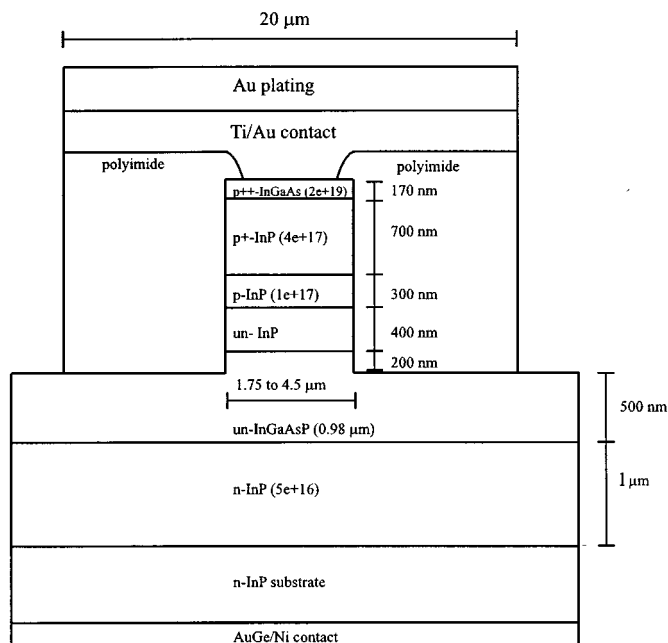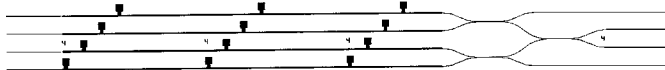
Fig. 2. Phase modulator structure.

Fig. 3. Schematic view of the PIC layout.

Fig. 4. Packaged and pigtailed PIC module

TABLE I
MEASURED FIBER-TO-FIBER LOSS ON PACKAGED AND PIGTAILED PIC
(IN DECIBELS)

In Out	I1	I2	I3	I4
O1	21	21	-	-
O2	25	24.5	24	31.5
O3	27	26	26	33
O4	-	-	21	27

In Out	O3
I1	27
I2	26
I3	26
I4	33

of 625 °C. Thus, we obtain a better control on the composition of the (low As content) quaternary guiding layer. The reactor pressure is 76 torr, except for the InGaAs contacting layer, where we use a higher pressure (700 torr) to obtain a higher doping level. The structure was grown on a $[100] + 2°$ off-oriented n-doped InP substrate.

After deposition of the different layers, the PIC waveguide structure is defined and etched (Fig. 3). The phase modulator section uses 2.25-μm-wide half-deeply (200 nm into the quaternary layer) etched waveguides, while the other waveguide structures (straight and bent waveguides and MMI sections) are deeply etched. The straight and bent waveguides have a ridge width of 2 μm, and the MMI's are 7-μm wide and 308-μm long.

First, an SiO_x layer and photoresist are deposited. The waveguide mask pattern (defined in the photoresist by photolithography) is transferred to the dielectric layer by $CF_4 : O_2$ plasma etching. The waveguide ridges are etched (half-deeply) by $CH_4 : H_2$ reactive ion etching (RIE). After a new lithography step leaving the phase modulator section covered, the MMI section is deeply etched. After removal of the remaining oxide layer, a polyimide and photoresist layer are spun over the sample. Via-holes are etched in the polyimide layer on top of the phase-modulator sections, and Ti–Au and Au layers are defined over the phase modulators for p-contacting. Finally, after removal of the polyimide layer and substrate thinning, AuGe–Ni is deposited on the substrate bottom as an ohmic back contact.

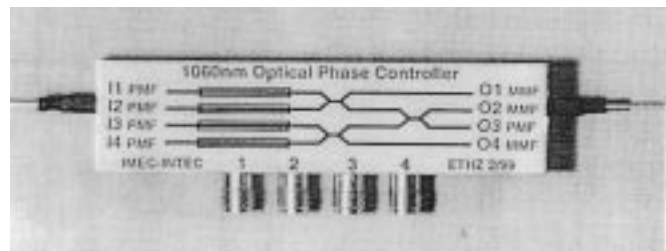After completion and preliminary testing, the PIC was pigtailed and packaged (Fig. 4). The input and output facets of the chip have been connected to arrays of four fibers each, consisting of four polarization maintaining fibers (PMF) at the input and 1 PMF (output channel 3) and 3 multimode fibers (MMF's) at the output side. The PMF connected output contains the antenna output signal; the other (MMF connected) output signals are minimized by controlling the phase modulators. For the optical connection to the PIC, the fibers are rotationally aligned and glued in Si V-groove arrays to achieve a precision in the submicrometer range. The fiber arrays are then polished, aligned to the waveguide arrays, and fixed. After mounting the PIC on a submount in the package, the phase modulators are wire bonded to transmission lines that lead to SMA connectors for applying the desired bias voltages. The optical fibers are strain relieved in the package sidewalls.

III. RESULTS

The results of the fiber-to-fiber loss measurements on the packaged and pigtailed module are given in Table I.

The total throughput for the output signal is approximately −27 dB, disregarding the results for input 4, which exhibits about 6-dB extra loss over the other inputs due to on-chip waveguide damage. 6 dB of the observed fiber-to-fiber throughput of −27 dB is due to the two 3-dB MMI couplers passed by every output signal, and the measurements also include 0.5–1-dB PMF connector loss, thus the actual fiber-to-fiber transmission loss is ∼20 dB. This applies when using output 3; the other output paths exhibit about 2-dB less loss, which can be attributed to the extra coupling loss to a PMF (at output 3) instead of that to a MMF as used for the other output paths. From a comparison between the losses in the different paths

TABLE II
OVERVIEW OF LOSS CONTRIBUTIONS FOR THE PACKAGED MODULE

	Loss (dB)
Fibre-chip coupling and reflection	2x6 = 12
On-chip Propagation (total path length = 8.55 mm)	4
MMI excess	2x1 = 2
Bend excess	1
Half-deep – deep excess	1
Total	20

TABLE III
FULL-WAVE VOLTAGE OF THE PIC'S PHASE MODULATORS AT
DIFFERENT BIAS VOLTAGES

Phase Modulator	$V_{2\pi}$ at 2.5 V	$V_{2\pi}$ at 5 V	$V_{2\pi}$ at 8.5 V
1	5.0	4.1	3.0
2	5.0	3.8	2.8
3	4.8	3.9	2.6
4	5.0	3.8	2.8

Fig. 5. Residual amplitude modulation of phase modulator

and measurements on individual component test structures, we obtain a contribution of these losses as presented in Table II.

The main contributions to the fiber-to-fiber total loss are fiber-chip coupling (10.5 dB) and facet reflection (1.5 dB) losses. The latter could be largely overcome by depositing a suitable AR coating on the chip facets, while the former can be strongly reduced by the application of tapered waveguide sections. Tapered waveguide sections were not included on the PIC, but have been manufactured and tested previously [5]. Applying an optimized AR coating and tapered waveguide sections at the chip facets could reduce the observed overall fiber-to-fiber losses by approximately 6 dB, taking into account approximately 8-dB fiber-chip coupling and reflection loss reduction, and 1-dB extra propagation loss per taper.

A very important section of the PIC is the phase-modulator section since this is responsible for generating the phase shifts required in the different paths to achieve constructive interference at the output port. Phase modulators are characterized by their phase —modulation efficiency, which expresses the phase shift as a function of the phase-modulator length and applied reverse-bias voltage. Table III gives the full-wave voltage $V_{2\pi}$, i.e., the voltage needed to achieve a phase shift of 2π, for the different phase modulators on the PIC and at different bias points.

Taking into account the length of the phase modulator sections (5.4 mm), this means that we have obtained phase modulation efficiencies of 13.3°/V/mm at 2.5-V reverse bias and 23.8°/V/mm at 8.5 V, respectively. Hence, a total phase shift of 5π can be achieved with a reverse bias voltage between 0–10 V (which is the safe operating range of the modulators).
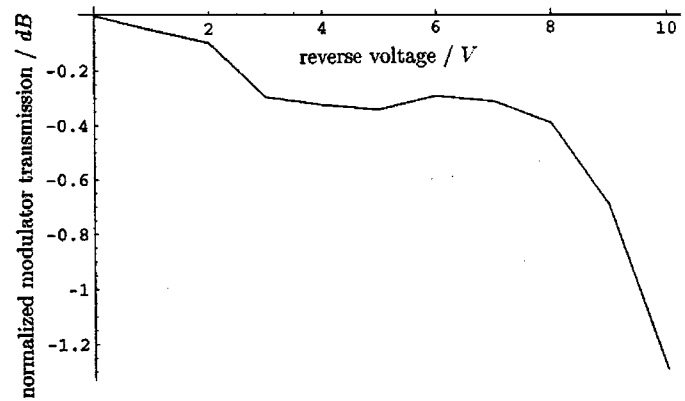
Since the phase modulators, besides changing the phase of the optical field, usually also cause an (unwanted) amplitude modulation, measurements of this residual amplitude modulation as a function of reverse bias voltage have also been performed. As can be seen from Fig. 5, the decrease in optical transmission is limited to less than 1.5 dB in the applied bias voltage range.

IV. CONCLUSION

We have demonstrated a 4×4 InGaAsP–InP PIC, suitable for phase control of 1.06-μm optical radiation. The PIC exhibits a total fiber-to-fiber loss of approximately 20 dB. The phase-modulator sections can accomplish a total phase shift of 5π with a maximum reverse bias voltage of 10 V. We believe that InP-based PIC's are a viable solution for optical phase control at 1.06 μm.

ACKNOWLEDGMENT

REFERENCES

[1] A. Kalmar, K. H. Kudielka, and W. R. Leeb, "Experimental demonstration of a self-tracking 16-aperture receive telescope array for laser inter-satellite communications," *Proc. SPIE*, vol. 3266, p. 70, 1998.

[2] B. Golubovic *et al.*, "Basic module for an integrated optical phase difference measurement and correction system," *IEEE Photon. Technol. Lett.*, vol. 7, pp. 649–51, MONTH 1995.

[3] W. K. Marshall and J. Katz, "Waveguide PIN junction electrooptic phase modulators: Theoretical analysis and design criteria," *Appl. Opt.*, vol. 24, no. 11, p. 1996, 1985.

[4] J. Vinchant *et al.*, "InP/GaInAsP guided-wave phase modulators based on carrier-induced effects: Theory and experiment," *J. Lightwave Technol.*, vol. 10, p. 63, Jan. 1992.

[5] J. Hendrix and G. Flamand *et al.*, "InP-based modulator array antennas at 1.06 μm," in *Proc. 10th Int. InP Related Mater. Conf.*, Tsukuba, Japan, May 1998, p. 687.